NANO LETTERS

pubs.acs.org/NanoLett

In Situ Observation of Reversible Nanomagnetic Switching Induced by Electric Fields

Todd Brintlinger,[†,‡] Sung-Hwan Lim,[‡,⊥] Kamal H. Baloch,[‡,§] Paris Alexander,[‡] Yi Qi,[‡] John Barry,[∥] John Melngailis,[∥] Lourdes Salamanca-Riba,[‡] I. Takeuchi,[‡] and John Cumings*[,‡]

[†]Naval Research Laboratory, Washington, D.C. 20375 and [‡]Department of Materials Science and Engineering, [§]Institute for Physical Science and Technology, and [∥]Department of Electrical and Computer Engineering, University of Maryland, College Park, Maryland 20742

ABSTRACT We report direct observation of controlled and reversible switching of magnetic domains using static (dc) electric fields applied in situ during Lorentz microscopy. The switching is realized through electromechanical coupling in thin film $Fe_{0.7}Ga_{0.3}/BaTiO_3$ bilayer structures mechanically released from the growth substrate. The domain wall motion is observed dynamically, allowing the direct association of local magnetic ordering throughout a range of applied electric fields. During application of ~7−11 MV/m electric fields to the piezoelectric $BaTiO_3$ film, local magnetic domains rearrange in the ferromagnetic $Fe_{0.7}Ga_{0.3}$ layer due to the transfer of strain from the $BaTiO_3$ film. A simulation based on micromagnetic modeling shows a magnetostrictive anisotropy of 25 kPa induced in the $Fe_{0.7}Ga_{0.3}$ due to the strain. This electric-field-dependent uniaxial anisotropy is proposed as a possible mechanism to control the coercive field during operation of an integrated magnetoelectric memory node.

KEYWORDS Multiferroic, magnetoelectric, domain wall, Lorentz, in situ

Modern electromagnetic theory firmly establishes a connection between electric and magnetic fields when either has an explicit time dependence, but magnetism and electricity generally do not couple as static fields. Nanostructures that induce such a coupling may prove an important technological tool, enabling spintronic[1] technologies such as magnetic random access memory (MRAM). Multiferroic systems are the focus of much current research seeking to realize engineered or nanostructured materials that directly couple static magnetic and electric fields through ferroelectric and ferromagnetic phases. Several strategies toward this end include magnetic control of ferroelectric polarization[2,3] and electrical control of a magnetic phase,[4] but the effects observed in natural multiferroics are generally very small and/or occur only at cryogenic temperatures. More promising results have come from heterostructure geometries where an interfacial interaction is exploited for electric-field-induced change in magnetic properties between a ferroelectric/piezoelectric layer and a magnetic layer.[5−9] Among them, a common method involves elastic coupling at an interface where strain transfer leads to a magnetoelectric behavior.[5−7]

Of particular interest from the application point of view are device architectures where electric field can be used to achieve switching of local magnetization.[9,10] Such effects might be used to provide direct electric field control over the direction of a magnetic bit for magnetic random-access memory. However, difficulty in precisely controlling the local magnetization switching and nontrivial characterization methods required to probe the effect have precluded detailed investigation of such individual switching behavior to date, and the previous studies have been unable to confirm a discrete switching of magnetic orientation with an appreciably large bistable region in applied electric field, as would be necessary for a memory element. Here, we demonstrate that through real-time imaging of magnetic domain structures, we can track and monitor the occurrence of individual magnetization switching events as the applied voltage is continuously varied and we supply our data here as still micrographs and in digital media as an annotated full-motion video (Supporting Information). Strain-mediated magnetoelectric coupling in unclamped ferromagnetic/ferroelectric bilayer structures is used to induce reversible switching. We observe two discrete magnetic states with a large region of bistability in electric field and no appreciable sensitivity outside this range. Accompanying OOMMF simulations and analysis of the observed change are in agreement with the estimated change in magnetic anisotropy due to inverse magnetostriction.

In the study of the magnetoelectric effect, proper choice of materials must also be supplemented with a suitable measurement technique to document the effect. To show ME coupling with sub-100-nm resolution, the scale at which they are envisioned for technological deployment, researchers have relied on high-resolution imaging techniques, such

* Corresponding author, cumings@umd.edu.

[⊥] Current address: Intel Portland Technology Development, Hillsboro, OR.

Received for review: 10/30/2009
Published on Web: 03/03/2010

DOI: 10.1021/nl9036406 | *Nano Lett.* **2010,** *10,* 1219–1223

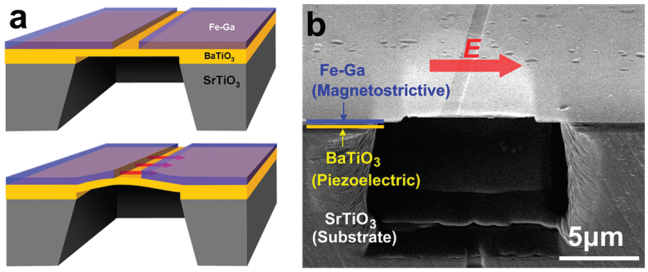

FIGURE 1. FeGa/$BaTiO_3$ thin film bilayer structure. (a) Schematic of device. Top image shows the sputter-deposited FeGa thin film with gap to form electrodes for application of electric field. $BaTiO_3$ is released from $SrTiO_3$ substrate in region of interest beneath patterned FeGa. Bottom image shows schematic representation of electric field (red arrows) and resulting mechanical response in piezoelectric $BaTiO_3$. (b) Scanning electron micrograph of device. Patterned FeGa film is shown on top of $BaTiO_3$, with $SrTiO_3$ substrate removed via focused ion beam milling. Electric field direction is shown schematically with red arrow.

as piezoelectric force microscopy,[11] magnetic force microscopy,[7,12] and/or X-ray magnetic circular dichroism photoelectron emission microscopy.[9] Previously, use of magneto-optical indicator films has also been reported as an effective means to observe magnetic domain wall motion in mechanically strained magnetostrictive thin films at a larger scale.[13] These previous methods all suffer from being slow and thus giving only a static picture of the magnetic structure or from having low spatial resolution (in the case of magneto-optical methods). The technique we use here is Lorentz microscopy, a form of transmission electron microscopy (TEM) providing sub-100-nm characterization of local in-plane magnetization over a wide field-of-view.[14,15] More importantly, Lorentz TEM allows the real-time video-rate imaging necessary to interrogate magnetic structure over a continuously varied range of applied electric fields.

We depict our composite thin film bilayer device in Figure 1. Shown schematically in a) and experimentally in b), an epitaxial ferroelectric (piezoelectric) layer of $BaTiO_3$ is combined with a polycrystalline ferromagnetic (magnetostrictive) layer of FeGa ($Fe_{0.7}Ga_{0.3}$) to form the core of our magnetoelectric device. We use polycrystalline FeGa thin films that were previously shown to display saturation magnetostriction of 100 ppm. The FeGa film is patterned into two conducting electrodes, which can directly apply electric fields to the $BaTiO_3$ layer. To ensure a full elastic response in the $BaTiO_3$ layer in the active device region, it is released from the $SrTiO_3$ substrate underneath using focused ion beam milling. As the electric field is applied, piezoelectric strain is developed in the $BaTiO_3$ layer near the gap region which in turn transfers the elastic strain to the FeGa film in this region. This removal of the $SrTiO_3$ substrate serves an additional function in making the system electron transparent, a necessary requirement for Lorentz microscopy.

We first characterize the FeGa film using magnetic field alone. Panels a, c, and d of Figure 2 show plan-view Lorentz-TEM images of the fabricated bilayer device in sequential order during the in situ application of magnetic fields. In

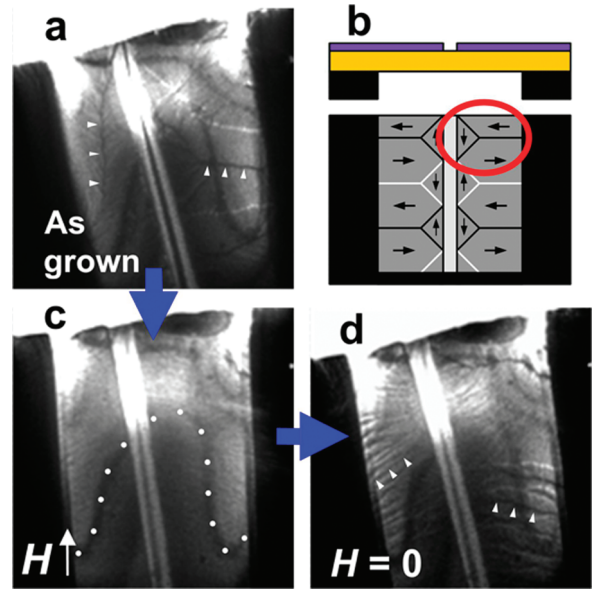

FIGURE 2. Magnetic response of thin film bilayer device. (a), (c), and (d) show plan-view Lorentz microscopy of device with varying magnetic fields applied. Blue arrows indicate order of operation. (b) A schematic of the device in side-view (top) and plan-view (bottom). The light and dark lines in the plan view are an idealized cartoon of the device with the domain walls separating domains with magnetization direction show by arrows. The red-circled region is depicted in Figure 3. (a) As-grown film on completed device. Lines of sharp dark and light contrast are domain walls. Ferromagnetic domains are oriented in all directions within FeGa film. Diffuse dark contrast indicates bend contours, not magnetic contrast., Magnetic domain walls are indicated with white triangles. (c) Film during application of large in-plane magnetic field (~500 Ga). No sharp contrast is evident as all domains collapse into single large ferromagnetic domain in the direction of applied field. White circles show Bragg-diffraction bend contours, which do not move under applied magnetic field. (d) Film after zeroing magnetic field. Ferromagnetic domains nucleate upon removal of large in-plane magnetic field, particularly along strained edges where bilayer structure meets the rigid substrate. White triangles show the new positions of magnetic domain walls.

Figure 2a, the film is in its as-grown state, with no specific magnetic history. To observe magnetic contrast, Lorentz microscopy captures changes in the imaging beam's phase, via the Lorentz force, as it interacts with the sample's local in-plane magnetization.[16] The interference created by this phase change will impart certain regions (domain walls) of the sample with light or dark contrast, depending on the magnetization of the sample and the focal length of the lens. The resulting contrast can be seen most illustratively in (a) as sharp light or dark lines. These are the walls between ferromagnetic domains with different local magnetization directions. The magnetic character of these contrast features can be verified by a simple variation of focus. Also visible are larger, diffuse lines of dark contrast (Bragg-diffraction bend contours) as well as bright regions near the edge of the device region (due to specimen thinning). These do not show strong contrast variation with focal length and are thus not magnetic in origin.

In Figure 2c, a large magnetic field has been applied in the plane of the FeGa film (H_c(FeGa) = ~200 Oe). Here, the

DOI: 10.1021/nl9036406 | *Nano Lett.* **2010,** *10,* 1219–1223

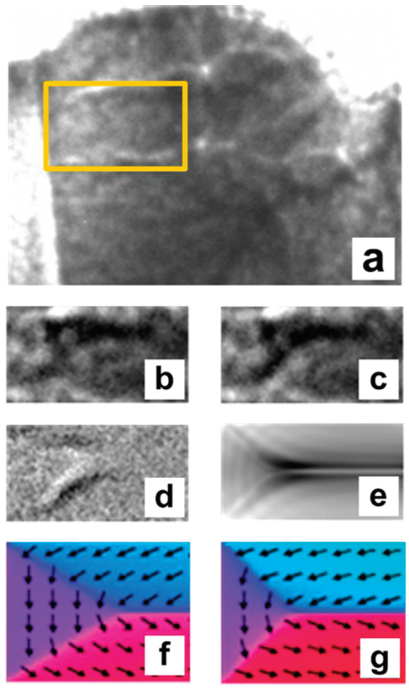

FIGURE 3. Reversible control of magnetic domain using static electric field, experiment, and simulation (red-circle region of Figure 2b). (a) Lorentz microscopy image of FeGa film with region-of-interest (yellow box) for magnetic domain motion. (b) and (c) Magnetic domain Lorentz image in low-electric-field state and high-electric-field state, respectively. (d) Difference image obtained by subtracting (c) from (b), showing motion of domain wall. (f) and (g) Local magnetic moments in object-oriented micromagnetic framework (OOMMF) simulation, prepared iteratively to match images (b), (c), and (d). Parts f and g show crystalline anisotropies of 0 and 25 kPa, respectively. (e) Simulation of (d) using contrast transfer function[16] and magnetization maps obtained from (f) and (g).

sharp lines of light and dark contrast disappear as the magnetic moment saturates in the direction of the applied magnetic field, leaving behind the other contrast features that are not magnetic in origin, as described above. In Figure 2d, the applied magnetic field of part c is removed, and the large, single magnetic domain relaxes into many smaller regions of local ferromagnetic order. Unlike the as-grown state of (a), the domain walls now have a preferred direction (all running roughly horizontal). This cycling establishes that the magnetic character of the FeGa film is intact following device fabrication and demonstrates the utility of Lorentz microscopy in observing local magnetization.

We then induce changes in local magnetization of the FeGa using electric field alone. Figure 3 shows the reversible control of magnetic domain motion induced by these static electric fields. These are still-frames of dynamic data recorded throughout application of electric fields, and an annotated full-motion video of this is provided as Supporting Information. Parts a−d represent the experimental confirmation of magnetoelectric coupling within the device, while parts e−g are simulations designed to understand this behavior. Part a is a Lorentz image of a device, zoomed as indicated by the red circle in Figure 2b. With the FeGa film used as metallic electrodes, electric field sweeps (±10 MV/m total in 0.2−0.5 MV/m steps) are performed during continuous observation of the device with Lorentz microscopy. Slowly varying Bragg-diffraction bend contours over a wide field-of-view indicate that strain is a continuous function of voltage because the $BaTiO_3$ is a membrane clamped by the substrate on three sides. Discrete magnetization switching events happen in addition to the observed strain, with a magnetic hysteretic effect due to local variations in magnetic order. The yellow box further zooms in on a region where particularly prominent reversible magnetization switching is observed. Similar switching features are observed in other samples and at other regions in this sample. This switching change is most readily characterized by domain wall motion, due to the pronounced contrast within the walls. Parts b and c show high-resolution, before-and-after Lorentz images of the yellow-boxed region in which domain wall motion occurred as a result of applied electric field. Note that many of the domain walls in the field of view exhibit no motion. This is expected, as a magnetostrictive uniaxial anisotropy is unable to impart any force upon the ubiquitous 180° domain walls, due to the symmetry of the magnetostriction. However, the induced anisotropy should cause a preference under applied voltage for domains with magnetic moment oriented horizontal in Figure 3 over those with vertical magnetic moment. This would produce a force on a 90° domain wall. Part d is a difference image of (c) and (d). Here, indeed, motion of a pair of 90° domain walls is seen as light/dark contrast. Thus, we observe similar magnetic domain response to that seen in Figure 2 with applied magnetic fields, but it originates under application of *dc electric fields*.

To understand the motion of these specific domain walls, we turn to simulations based on the object-oriented micromagnetic framework (OOMMF).[17] Figure 3e is a simulation of the experimental difference image seen in (d). In (e), contrast is produced according to the local magnetic moments for two different domain wall configurations, seen in (f) and (g). To obtain both (f) and (g), OOMMF simulations were run using saturation magnetization (M_{sat}) = 1.360×10^6 A/m, exchange stiffness (A) = 1.4×10^{-11} J/m, and thickness (t) = 30 nm, values independently measured for our FeGa films. A uniaxial inverse-magnetostriction anisotropy constant (K, in pascals) was then allowed to vary in 5 kPa steps. Parts f and g give the difference image, seen in (e), most closely resembling the experimental images and representing a uniaxial magnetostriction anisotropy of 25 kPa. Differences in simulated and experimental images are mostly attributable to approximations in the contrast transfer function and unoptimized Lorentz simulations. However, the general bright-dark contrast is similar and the angles of the lower domain wall are matched to within ±3°. Thus, electrically induced nanomagnetic switching can be described by a variation in the uniaxial magnetic anisotropy.

This nanomagnetic switching, observed in Figure 3 and described above, has been observed in all devices measured

DOI: 10.1021/nl9036406 | *Nano Lett.* **2010,** *10,* 1219–1223

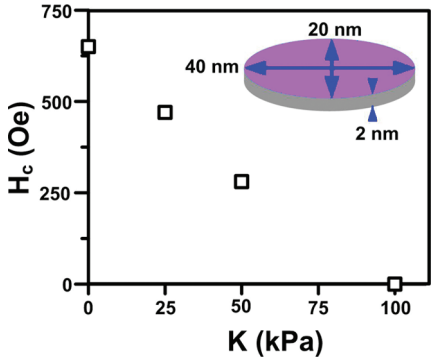

FIGURE 4. Magnetoelectric memory node. Inset shows a thin film ellipsoid of magnetostrictive material. With locally modulated strain, the anisotropy of the element can be controlled. Derived using OOMMF simulations and the parameters developed within this work, the graph plots the coercive field versus strain-induced uniaxial anisotropy. This shows how such a material could be exploited for improved magnetic random access memory.

(three total), with similar fields (~7−11 MV/m) required to move domains. Samples show multiple regions in which domain wall motion occurs, and this motion is repeatable and reversible to within ±1 MV/m for a given domain. To quantitatively understand the effect of magnetoelectrically coupled nanomagnetic switching, we begin with the piezoelectric layer. We use the piezoelectric coefficient of $BaTiO_3$ d_{33}, of ~50 pm/V for thin films.[18] Taking this value along with the applied field, we obtain a strain, $\varepsilon_{BTO} = (50\ pm/V) \times (10\ MV/m) = 500 \times 10^{-6}$. Because the $BaTiO_3$ layer (200 nm) is much thicker, we conclude that the strain is entirely passed to the interfacially coupled FeGa film (30 nm), such that $\varepsilon_{BTO} = \varepsilon_{FeGa} = 500 \times 10^{-6}$. A Young's modulus of 140 GPa for FeGa[19] then leads to $\sigma_{FeGa} = \varepsilon_{FeGa} \times E_{FeGa} = (500 \times 10^{-6}) \times (140\ GPa) = 70$ MPa of stress. This stress can then be combined with known values for magnetostriction,[20] to arrive at an induced crystalline anisotropy of: $K = 3/2 \times \lambda_{FeGa} \times \sigma_{FeGa} = (3/2) \times 100\ ppm \times 70\ MPa = 10$ kPa. Because OOMMF simulation does not account for local disorder, it overestimates the energy difference between the two micromagnetic states, which are possibly in a two-state double-well configuration. Given the uncertainties in both simulation and experiment, a factor of 2 difference is in good agreement with the value obtained through micromagnetic simulation of the Lorentz images, providing confirmation for the magnetoelectric origin of the electric-field-induced domain wall motion.

Figure 4 describes a technological implementation of this electrically tunable uniaxial anisotropy. Demonstrated and proposed MRAM technologies make use of either Oersted fields[21,22] or spin-torque effects,[23,24] both of which require substantial current densities for writing or erasing magnetic elements. We propose an MRAM mechanism that reduces the current density (and thus power density) required for the switching, by application of a static electric field simultaneously to reduce the anisotropy barrier for switching the relevant magnetic element. The magnetostrictive switching mechanism that we report here cannot by itself produce a switching between the usual parallel and antiparallel magnetic configurations used in MRAM devices as the binary 1 and 0 states, due to the symmetry of the magnetostrictive anisotropy. Nevertheless, magnetostriction can be used to reduce the anisotropy of a selected MRAM node in situ, thus reducing the current needed to switch the element by the usual methods. Figure 4 plots the coercive field, H_c, versus uniaxial anisotropy, K, for a $20 \times 40 \times 2$ nm^3 ellipsoid of FeGa thin film (shown in the inset), determined using OOMMF along with parameters derived from this work. These dimensions would be in the range of what might be used for the writable magnetic layer in an MRAM device.[21,22] Using an electric field to control the magnetic anisotropy, which in turn controls the coercive field, it is envisioned that the nanomagnetic ellipsoid can be changed from a hard magnet to a soft magnet by varying voltage.[25] This voltage-controlled anisotropy also affords a means by which global behaviors may be forced into compliance despite variations in individual nodes. Large arrays of nodes could have their collective coercive fields reduced to near zero by a universally applied voltage, allowing simultaneously reset through applied magnetic and electric fields. This voltage-controlled switching between hard and soft magnets thus provides a new avenue in the contradictory design needs of magnetically based memories, which simultaneously require large coercive fields for long-term fidelity and small coercive fields for efficient switching.

Thus, we demonstrate use of a static electric field to switch the local magnetization within a bilayer thin film device, with the motion of domain walls interrogated by Lorentz microscopy. Simulations show the magnetic anisotropy of the FeGa film varying from zero up to 25 kPa due to applied electric fields of ~7−11 MV/m, and this fact can be exploited for a nanometer-scale magnetoelectric memory node. Continuing research will incorporate more complex geometries for the probing of similar magnetoelectric systems, and the direct application of strain (via mechanical interactions) to the magnetostrictive films may help to identify improved means for controlling the magnetic domains.

Acknowledgment. Authors acknowledge funding from NSF MRSEC (DMR 0520471), ONR-MURI N000140610530, ARO W911NF-07-1-0410, and NEDO. We acknowledge useful discussions with M. Wuttig and S. E. Lofland, and we acknowledge S. Kennedy for technical assistance. We acknowledge the support of the Maryland NanoCenter and its NISPLab and FabLab. The NISPLab is supported in part by the NSF as a MRSEC Shared Experimental Facility.

Note Added after ASAP Publication. The Acknowledgement section was modified in the version of this paper published ASAP March 3, 2010; the corrected version published ASAP March 12, 2010.

DOI: 10.1021/nl9036406 | *Nano Lett.* **2010,** *10,* 1219–1223

Supporting Information Available. Additional information on thin film deposition, patterning electrodes, and TEM sample preparation and a video showing magnetization switching events. This material is available free of charge via the Internet at http://pubs.acs.org.

REFERENCES AND NOTES

(1) Žutić, I.; Fabian, J.; Das Sarma, S. *Rev. Mod. Phys.* **2004**, *76* (2), 323.

(2) Kimura, T.; Goto, T.; Shintani, H.; Ishizaka, K.; Arima, T.; Tokura, Y. *Nature* **2003**, *426* (6962), 55–58.

(3) Hur, N.; Park, S.; Sharma, P. A.; Ahn, J. S.; Guha, S.; Cheong, S. W. *Nature* **2004**, *429* (6990), 392–395.

(4) Lottermoser, T.; Lonkai, T.; Amann, U.; Hohlwein, D.; Ihringer, J.; Fiebig, M. *Nature* **2004**, *430* (6999), 541–544.

(5) Sahoo, S.; Polisetty, S.; Duan, C.-G.; Jaswal, S. S.; Tsymbal, E. Y.; Binek, C. *Phys. Rev. B: Condens. Matter Materi. Phys.* **2007**, *76* (9), No. 092108-4.

(6) Overby, M.; Chernyshov, A.; Rokhinson, L. P.; Liu, X.; Furdyna, J. K. *Appl. Phys. Lett.* **2008**, (19), 92.

(7) Chung, T. K.; Keller, S.; Carman, G. P. *Appl. Phys. Lett.* **2009**, (13), 94.

(8) Molegraaf, H. J. A.; Hoffman, J.; Vaz, C. A. F.; Gariglio, S.; Marel, D. v. d.; Ahn, C. H.; Triscone, J.-M. *Adv. Mater.* **2009**, *21*, 1–5.

(9) Chu, Y. H.; Martin, L. W.; Holcomb, M. B.; Gajek, M.; Han, S. J.; He, Q.; Balke, N.; Yang, C. H.; Lee, D.; Hu, W.; Zhan, Q.; Yang, P. L.; Fraile-Rodriguez, A.; Scholl, A.; Wang, S. X.; Ramesh, R. *Nat. Mater.* **2008**, *7* (6), 478–482.

(10) Zavaliche, F.; Yang, S. Y.; Zhao, T.; Chu, Y. H.; Cruz, M. P.; Eom, C. B.; Ramesh, R. *Phase Transitions* **2006**, *79* (12), 991–1017.

(11) Shafer, P.; Zavaliche, F.; Chu, Y. H.; Yang, P. L.; Cruz, M. P.; Ramesh, R. *Appl. Phys. Lett.* **2007**, (20), 90.

(12) Chung, T. K.; Carman, G. P.; Mohanchandra, K. P. *Appl. Phys. Lett.* **2008** (11), 92.

(13) Shull, R. D.; Quandt, E.; Shapiro, A. T.; Glasmachers, S.; Wuttig, M. *J. Appl. Phys.* **2004**, *95* (11), 6948–6950.

(14) Chapman, J. N. *J. Phys. D: Appl. Phys.* **1984**, *17* (4), 623-&.

(15) Fuller, H. W.; Hale, M. E. *J. Appl. Phys.* **1960**, *31* (2), 238–248.

(16) Williams, D. B.; Carter, C. B., *Transmission electron microscopy: a textbook for materials science*; Plenum Press: New York, 1996; Vol. xxvii, p 729.

(17) Donahue, M. J.; Porter, D. G. *OOMMF User's Guide v1.0*; NIST: Gaithersburg, MD, 1999.

(18) Zheng, H.; Wang, J.; Lofland, S. E.; Ma, Z.; Mohaddes-Ardabili, L.; Zhao, T.; Salamanca-Riba, L.; Shinde, S. R.; Ogale, S. B.; Bai, F.; Viehland, D.; Jia, Y.; Schlom, D. G.; Wuttig, M.; Roytburd, A.; Ramesh, R. *Science* **2004**, *303* (5658), 661–663.

(19) Wuttig, M.; Dai, L. Y.; Cullen, J. *Appl. Phys. Lett.* **2002**, *80* (7), 1135–1137.

(20) Hattrick-Simpers, J. R.; Hunter, D.; Craciunescu, C. M.; Jang, K. S.; Murakami, M.; Cullen, J.; Wuttig, M.; Takeuchi, I.; Lofland, S. E.; Benderksy, L.; Woo, N.; Van Dover, R. B.; Takahashi, T.; Furuya, Y. *Appl. Phys. Lett.* **2008**, (10), 93.

(21) Tehrani, S.; Slaughter, J. M.; Deherrera, M.; Engel, B. N.; Rizzo, N. D.; Salter, J.; Durlam, M.; Dave, R. W.; Janesky, J.; Butcher, B.; Smith, K.; Grynkewich, G. *Proc. IEEE* **2003**, *91* (5), 703–714.

(22) DeBrosse, J.; Gogl, D.; Bette, A.; Hoenigschmid, H.; Robertazzi, R.; Arndt, C.; Braun, D.; Casarotto, D.; Havreluk, R.; Lammers, S.; Obermaier, W.; Reohr, W. R.; Viehmann, H.; Gallagher, W. J.; Muller, G. *IEEE J. Solid-State Circuits* **2004**, *39* (4), 678–683.

(23) Katine, J. A.; Albert, F. J.; Buhrman, R. A.; Myers, E. B.; Ralph, D. C. *Phys. Rev. Lett.* **2000**, *84* (14), 3149–3152.

(24) Albert, F. J.; Katine, J. A.; Buhrman, R. A.; Ralph, D. C. *Appl. Phys. Lett.* **2000**, *77* (23), 3809–3811.

(25) Novosad, V.; Otani, Y.; Ohsawa, A.; Kim, S. G.; Fukamichi, K.; Koike, J.; Maruyama, K.; Kitakami, O.; Shimada, Y. *J. Appl. Phys.* **2000**, *87* (9), 6400–6402.

DOI: 10.1021/nl9036406 | *Nano Lett.* **2010,** *10,* 1219–1223